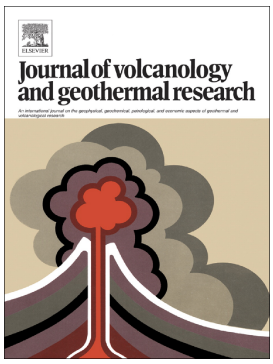

Multiscale and multitemporal surface temperature monitoring by satellite thermal infrared imagery at Mayon Volcano, Philippines

Hai-Po Chan, Kostas Konstantinou

PII: S0377-0273(19)30549-9

DOI: https://doi.org/10.1016/j.jvolgeores.2020.106976

Reference: VOLGEO 106976

To appear in: *Journal of Volcanology and Geothermal Research*

Received date: 16 October 2019

Revised date: 3 June 2020

Accepted date: 13 June 2020

Please cite this article as: H.-P. Chan and K. Konstantinou, Multiscale and multitemporal surface temperature monitoring by satellite thermal infrared imagery at Mayon Volcano, Philippines, *Journal of Volcanology and Geothermal Research* (2020), https://doi.org/10.1016/j.jvolgeores.2020.106976

Multiscale and Multitemporal Surface Temperature Monitoring by Satellite Thermal Infrared Imagery at Mayon Volcano, Philippines

Hai-Po Chan * and Kostas Konstantinou

Department of Earth Sciences and Graduate Institute of Geophysics, National Central University, Taoyuan City, Taiwan; haipochan@g.ncu.edu.tw; kkonst@cc.ncu.edu.tw

* Correspondence: haipochan@g.ncu.edu.tw; Tel.: +886-3-422-7151 ext. 65636

Abstract:

Mayon Volcano on eastern Luzon Island is the most active volcano in the Philippines. The high level of vulnerability to volcanic hazards is apparent since Mayon is surrounded by eight cities and municipalities with a total population of approximately one million inhabitants. Thus there is an urgent need to develop and expand reliable and affordable long-term methods in volcano monitoring. Despite abundant open access satellite dataset archives, satellite remote sensing has been underutilized in Mayon's hazard mapping and monitoring system. Here, we perform monitoring analysis on a nineteen-year time series of Land Surface Temperature (LST) obtained from satellite thermal infrared images. Both ASTER (Advanced Spaceborne Thermal Emission and Reflection Radiometer) thermal imagery (with 90 meters spatial resolution) and MODIS (Moderate Resolution Imaging Spectroradiometer) LST products (1 km spatial resolution) are used for the analysis. The Ensemble Empirical Mode Decomposition (EEMD) is applied as

the decomposition tool to extract components of different timescales from the LST time series. Physical interpretation of decomposed LST components at various periods are explored and compared with Mayon's eruption records. Specifically, the LST annual period component is compared to regular annual cycle air temperature. Results show that LST annual period component tends to lose its regularity following an eruption. The dissimilarity of the two time series has been taken as an indicator of volcanic restlessness. Trends of different timescales based on LST components have been constructed, which all indicate the rising trend. This means that Mayon volcano will remain restless in the future decades. This study presents the advantages and effectiveness of satellite remote sensing on volcanic monitoring.

Keywords: Mayon Volcano; Land Surface Temperature (LST); Thermal Infrared (TIR); Ensemble Empirical Mode Decomposition (EEMD); ASTER; MODIS

Highlights:

- Two-decade-long surface temperature at Mayon retrieved from MODIS and ASTER
- Components of various timescales extracted from the MODIS LST time series
- LST annual period component loses its regularity after eruptions
- Increasing secular trend points to future volcanic restlessness at Mayon

1. Introduction

On the Earth, at any given moment, there are at least 20 volcanoes actively erupting somewhere. Globally there are around 1,500 active volcanoes that have erupted in the Holocene, excluding the volcano belt of the ocean floor. Around 500 of them have erupted in documented history. Many of them are distributed along the Pacific Rim (i.e., Ring of Fire) (USGS, 2013). Volcanoes in the Philippines belong to the western part of the Pacific Rim, which resulted from the tectonic collision between the Philippine Sea Plate and the continental Eurasian Plate. The Philippine Institute of Volcanology and Seismology (PHIVOLCS) has reported 23 active volcanoes in the Philippines, 21 of which have historical eruptions. Among them, Mayon Volcano is the Philippines' most active volcano.

Mayon Volcano is located in the eastern part of Luzon Island in the Philippines. It is a symmetric stratovolcano rising to 2,462 m with the upper slopes of 35–40° and a small summit crater at the top (Figure 1). The historical eruptions are mostly basaltic-andesitic and their types range from Strombolian to basaltic Plinian (Castillo and Newhall, 2004). During typical eruptions lava flows are mainly produced from the central conduit and extended far down to the surrounding flanks. Pyroclastic flows and mudflows often sweep down the ravines (roughly 40 of them) from the summit and cause severe devastation in the populated lowland areas. Mayon is the most famous of the active volcanoes of the Philippines for its frequent eruptions that repeatedly triggered large scale evacuations. It has 64 displayed eruptions between 1616 and 2019 (GVP, 2013). The latest eruption

occurred on January 13, 2018 and is continuing until now. Mayon's deadliest eruption occurred on February 1, 1814, which claimed more than two thousand lives. Mayon's longest uninterrupted eruption occurred on June 23, 1897 (Volcanic Explosivity Index; VEI=4), in which a seven-day fire rain occurred from June 23 through 30. Over 400 people were killed by lava, ash, steam and falling debris or hot rocks in this eruption (Davis, 2010). Most recent disaster is the 1993 eruptions, in which a phreatic explosion occurred without any precursors and killed 77 people (Catane et al., 2001). PHIVOLCS has thus established a 6 km radius permanent danger zone at Mayon as a precaution against similar explosions. Recent activity of Mayon is characterized by pyroclastic flows, mud flows and ash falls with a repose period of several days to a few years (Maeda et al., 2015).

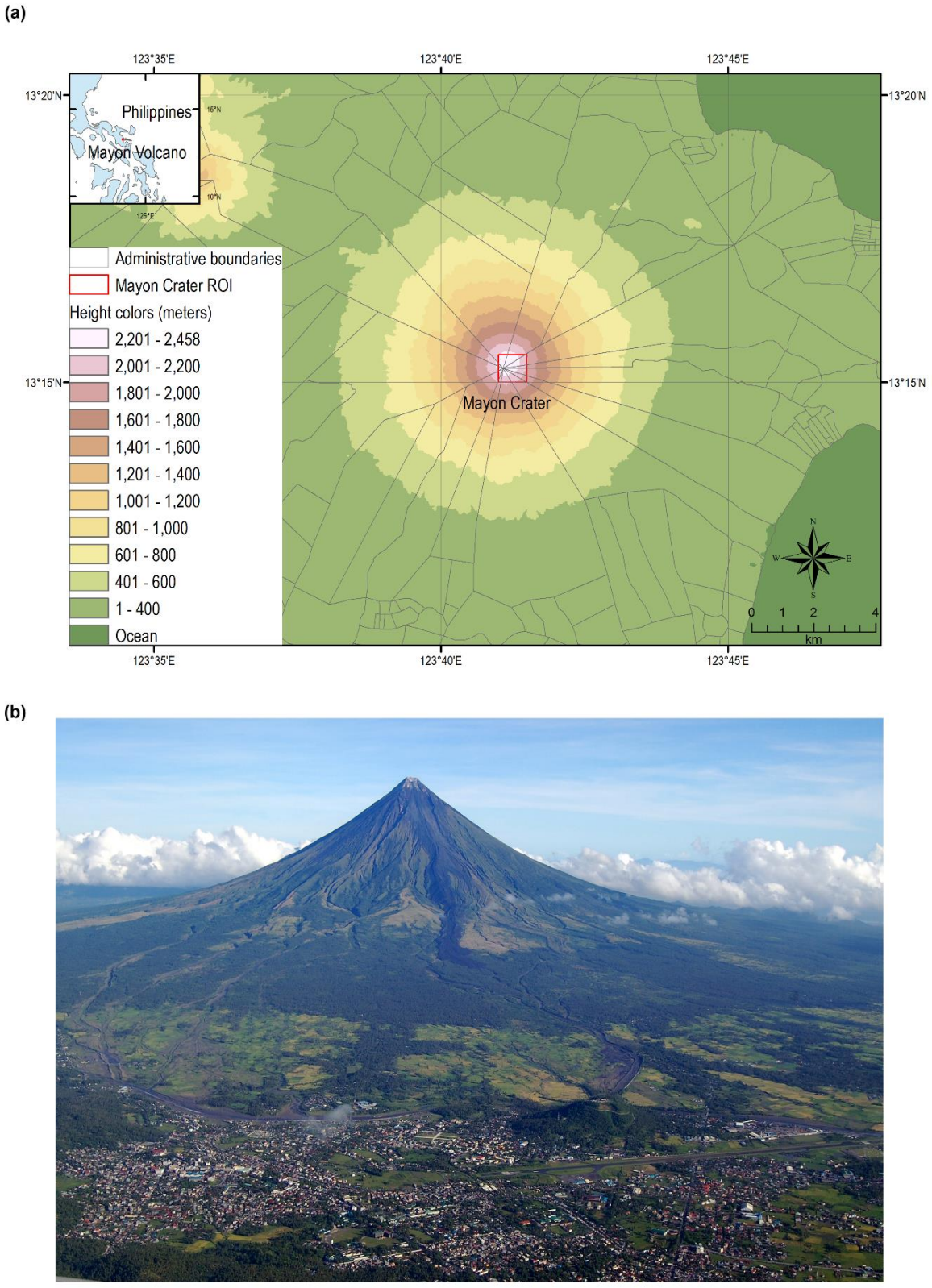

Figure 1. (a) Geography and DEM map of Mayon volcano, Philippines. Volcano crater region of interest (ROI) and administrative boundaries are indicated. (b) Aerial view of Mt. Mayon which is the most active volcano in the Philippines (By

Dexbaldon-Own work, CC BY-SA 4.0, https://commons.wikimedia.org/w/index.php?curid=43882874). Note the dense cluster of residences at the foot of the volcano.

Volcanic eruptions are fierce natural disasters for they may cause simultaneously numerous geologic and hydrologic hazards. Monitoring and assessment of volcanic activity is thus vital. Besides on site monitoring systems, satellite remote sensing provides many benefits for various volcano monitoring applications globally. For instance, satellite based Interferometric Synthetic Aperture Radar (InSAR) is an effective monitoring technology to detect and measure volcanic deformation before volcanic eruptions (Chadwick et al., 1988; Chaussard and Amelung, 2012; Rivera et al., 2015). Satellite remote sensing technologies have increased our ability to better monitor and understand the working mechanism of volcanoes and to compare volcanoes in alternative ways which are not feasible with in situ observations (Gupta, 2017; Pyle et al., 2013; Tokunaga and Thuy, 2000; Wooster et al., 2013). Satellite remote sensing techniques have been extensively used in recent decades for monitoring volcanoes worldwide and yielded promising results (Blackett, 2013; Blackett, 2015; Bull and Buurman, 2013; Delle Donne et al., 2010; Ewert et al., 2005; Flynn et al., 2001; Kisei et al., 2008; Roberti et al., 2018; Slob et al., 1998; Webley et al., 2008; Wright et al., 2002).

Mayon volcano is surrounded by the eight cities and municipalities (i.e., Legzpi, Daraga, Camalig, Guinobatan, Ligao, Tabaco, Malilipot, and Santo Domingo) with a total of approximately one million inhabitants and a Population

Exposure Index (PEI) of 6 (UNDRR, 2015). Monitoring volcanic activity in this area is thus of extreme importance. Compared to the existing in situ observation and on site monitoring at Mayon Volcano Observatory (MVO), satellite remote sensing technologies provide promising options, since the advantages of remote sensing include the ability to acquire information over large areas and also to observe and monitor surface objects on a systematic basis over time. Here we use sensors of the Terra/Aqua satellite (launched since 1999) from the National Aeronautics and Space Administration (NASA) and United States Geological Survey (USGS). We aim to present a multiscale and multitemporal monitoring analysis based on a two decade LST time series from ASTER (Advanced Spaceborne Thermal Emission and Reflection Radiometer) and MODIS (moderate resolution imaging spectroradiometer) satellite retrieved thermal infrared (TIR) imagery. We applied the Ensemble Empirical Mode Decomposition (EEMD) method to extract components of different timescales from the LST time series, and explored the physical interpretation of decomposed LST components at various periods compared with Mayon's eruption records. Based on the results we argue for the systematic integration of the satellite remote sensing approach into governmental hazard mapping and monitoring systems.

2. Materials and Methods

Free access satellite imagery from space agencies around the world are abundant and growing rapidly. To date, over a dozen of earth observation data sources are available to the public at no cost. Among them, NASA and USGS,

European Space Agency (ESA), and Japan Aerospace Exploration Agency (JAXA) are the three major imagery providers. In this study, we have used considerable amount of imagery from NASA and USGS owing to NASA's grant pioneer work on earth observation missions and the relative long-term imagery archives (since 1970s). Satellite thermal infrared imageries at Mayon Volcano for the period 2000–2019 (two decades) have been selected in imagery archives based on the image quality assessment (mainly on cloud contamination). Specifically, ASTER imagery with 90 m spatial resolution and MODIS LST products with 1 km spatial resolution are used for volcano monitoring purposes in this research. These two imagery datasets are complementary because MODIS imagery has high temporal but low spatial resolution, and ASTER imagery has high spatial but low temporal resolution (Bindhu et al., 2013; Bonafoni, 2016; Weng et al., 2014). Both MODIS and ASTER LST products are analysis-ready.

2.1. LST Products

This study uses both ASTER and MODIS imagery. ASTER Thermal imagery has a 90 m pixel size but it suffers from the relative scarcity of the dataset (one imagery per 16 days). However, MODIS supplies imagery subdaily at a 1 km spatial resolution and can be better used for monitoring purpose. The nighttime MODIS 8-day average LST data (Product ID: MOD11A2, MYD11A2) from March, 2000–April, 2019 at Mayon crater was selected. The MOD11A2 and MYD11A2 products are the 8-day average per pixel daily land surface temperature. The daily LST is calculated from the night LST algorithm based on nighttime observations in

MODIS TIR bands (Wan, 2014; Wan and Li, 1997). According to the theoretical description of LST calculation in the MODIS Land-Surface Temperature Algorithm Theoretical Basis Document (LST ATBD), MODIS team has implemented the generalized split-window algorithm and the day/night algorithm to retrieve LST after comprehensive numerical simulations and analysis. General concerns relevant to the validation of retrieved LST, including optical properties, night dew problem, thermal inertia, and cloud cover, as well as uncertainty estimation have been addressed in the algorithms (Wan, 1999). The accuracy of the released LST product is better than 1°K (0.5°K in most cases) based on the accuracy statement from MODIS land team of NASA.

The 8-day average LST product has the benefit of averaging out the cloud cover occurrence over 8 days and increasing the dataset reliability in the imagery. It has a significant advantage over ASTER imagery which only has a 16-day repeat coverage and is frequently contaminated by clouds. However, the 1km pixel size causes the thermal feature to represent a lower percentage of the pixel size and therefore depict the temperature less accurately. To illustrate the usefulness and relevance of a 1 km spatial resolution, the exemplary MODIS LST images on the Mayon volcanic zone are shown in Figure 2.

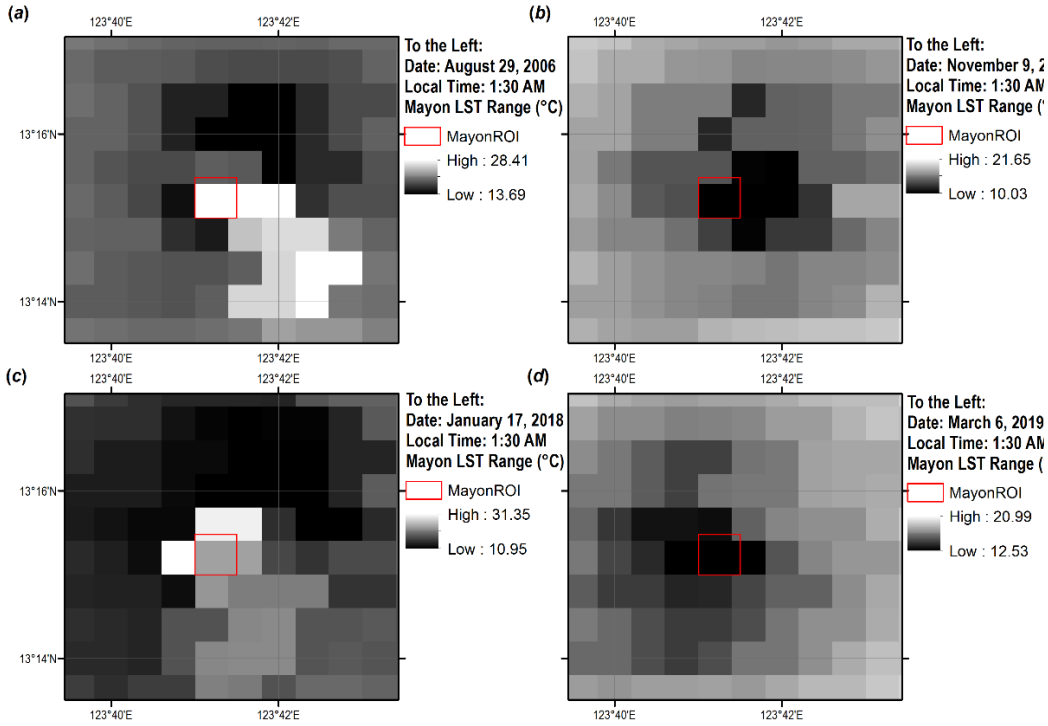

Figure 2. Example of MODIS LST images (Product ID: MOD11A2) with 1 km spatial resolution on Mayon volcano. Areas of Mayon crater (one pixel) are illustrated by red color polygonal region. Panel (a) and (c) present higher temperature; panel (b) and (d) show lower temperature at the volcanic area.

2.2. Ensemble Empirical Mode Decomposition (EEMD)

The EEMD is an empirical signal processing method that is used to extract physically meaningful information from nonstationary and nonlinear signals (Huang et al., 1998; Huang et al., 2003; Wu and Huang, 2009). Generally, traditional signal processing methods are mostly based on the assumptions of linearity and stationarity. Until recently, some mathematical methods have been developed to deal with either nonstationary or nonlinear signals. However, many situations in

real life require engineers and scientists to deal with nonstationary and nonlinear signals simultaneously. The EEMD provides an effective solution to the above mentioned issue. The EEMD is capable of dealing both with nonstationary and nonlinear signals, especially for the alternative relations in time, frequency and energy domain. In many cases, the EEMD is used to extract physical meaning from data to better interpret physical phenomena and to solve engineering problems (Cheng et al., 2015; Zhang et al., 2019).

In this study the EEMD is used to decompose MODIS LST time series into different simple components, i.e., the simple oscillatory mode which is called intrinsic mode function (IMF) in the time-domain. EEMD is an adaptive data decomposition method which is based on the nature of the data (i.e., its basis functions are derived from the data). In contrast, most typical data decomposition methods have an a priori basis (such as trigonometric functions in Fourier analysis; base wavelet in Wavelet transform), and they are not adaptive (Huang and Wu, 2008). With EEMD, the LST time series can be divided into a few intrinsic mode functions (IMFs), in which each IMF is corresponding to a certain physical meaning. Specifically, the LST decomposition results (i.e., IMFs) form a complete and orthogonal set of the original LST time series (Huang et al., 1998; Huang and Wu, 2008; Huang et al., 2009; Nunes and Deléchelle, 2009; Wang et al., 2014).

3. Results

It is necessary to confirm that the positive thermal anomaly is not caused by land use or land cover changes in the Mayon area before presenting the results. The

crater area, where LST is extracted from, is within the Permanent Danger Zone (PDZ) of Mayon defined by PHIVOLCS. It is the area of lava flow extending 6 km downward from the volcano's crater. The area of 6 km from the crater of Mayon volcano is almost all occupied by the tropical grass, wood, and brushwood. The outward extension of the lava flow hazard zone (about 12 km from the summit) is the pyroclastic hazard zone. Thus the High Danger Zone (HDZ) including the area between 6 km and 10 km downward from the volcano's crater was defined (JICA, 2006). Mayon's eruptions are active and long-standing, for instance, the most recent significant eruption during early 2018 features weak "lava fountaining", i.e. involved fresh lava arriving in the summit area. Early in February 2020, "crater glow" has been detected at the summit crater that is likely caused by hot magmatic gases heating the overlying atmosphere. This puts forward the possibility that remnant magma may be quietly rising to the shallow levels of the edifice. Previous geomorphological study and continuous observation on the distribution of lava flow and pyroclastic flow deposits for Mayon volcano over the study period show that no significant land use or land cover changes have occurred at the crater area (GVP, 2013; PHIVOLCS, 2020; Westen, 1994).

MODIS supplies imagery of 1 km spatial resolution subdaily. So the MODIS 8-day average nighttime dataset from March, 2000–April, 2019 at Mayon crater is used for the LST time series analysis. Figure 3 illustrates the nighttime MODIS 8-day average LST of Mayon crater (specified crater ROI in Figure 1a) from 2000–

2019. This two-decade LST time series displays the thermal variations caused by the volcanic activity.

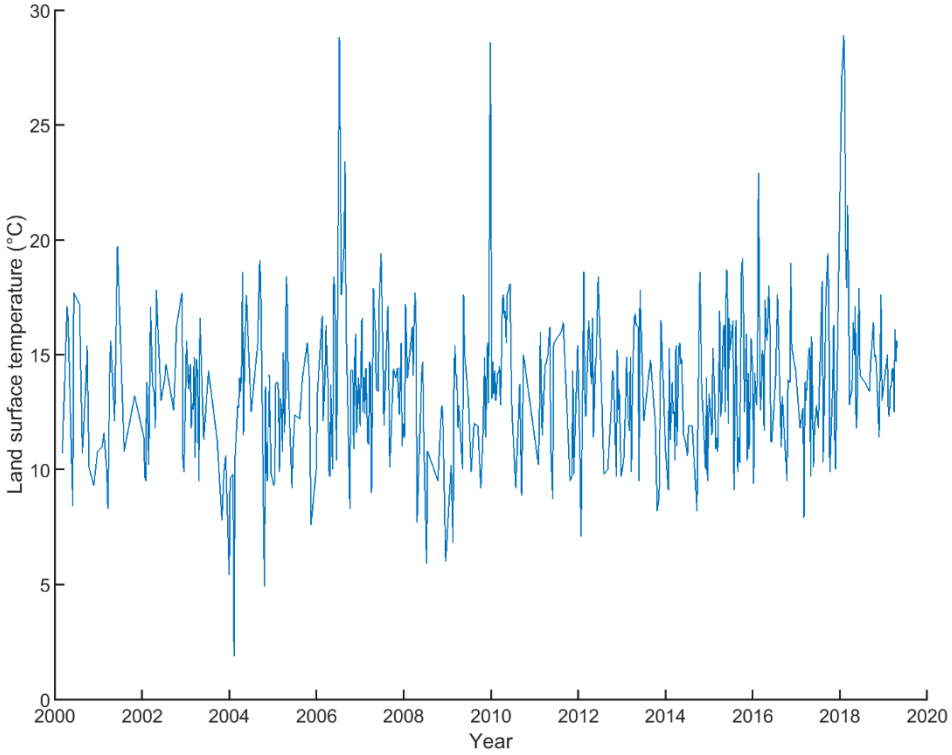

Figure 3. Illustration of the nighttime 8-day average LST from MODIS at Mayon crater from March, 2000 to April, 2019. Not all 8-day timeline points have an available dataset. The gaps in the dataset are probably caused by the heavy cloud cover. They indicate that there are no clear images available in this volcano area even after eight continuous days.

MODIS LST time series from 2000 to 2019 (in Figure 3) contains rich underlying physical characteristics. Fourier and Wavelets transforms can be good tools to extract hidden information. However, considering the nonstationary and nonlinear characteristics of LST time series, EEMD is more preferable. Thus EEMD has been

applied to get the MODIS LST components in the time-frequency-energy domain. The time series of MODIS LST is the product of 8-day average LST, and despite contamination by cloud coverage, the data availability is acceptable for such an analysis (around 800 data points for the period of March, 2000–April, 2019). The resulting MODIS LST and its EEMD decomposition are illustrated in Figure 4.

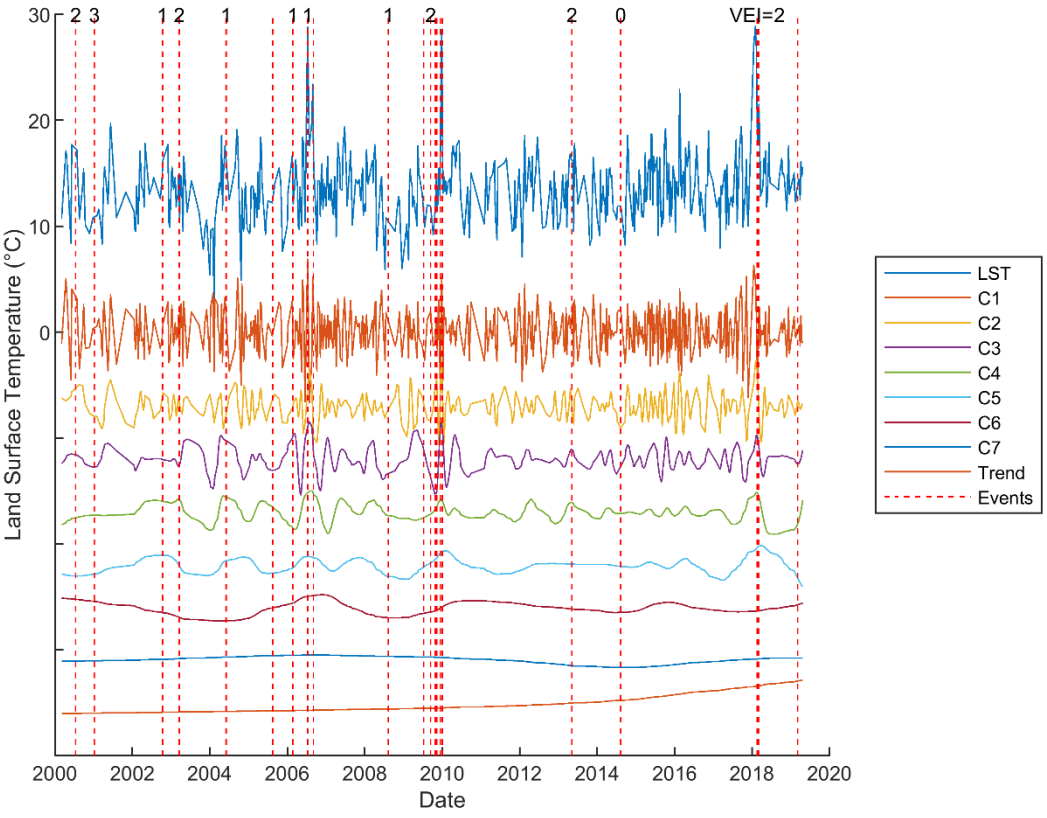

Figure 4. MODIS LST and its EEMD decomposition from 2000–2019 for Mayon crater. The MODIS LST is indicated by the top blue line and EEMD components (IMFs; C1–C7) are beneath. The red color vertical dashed lines represent recorded volcanic unrest periods or eruptions. Events dataset are from the online Volcano Bulletin of PHIVOLCS (available at https://www.phivolcs.dost.gov.ph/) and eruptive history database of global

volcanism program, Smithsonian Institution (available at https://volcano.si.edu/volcano.cfm?vn=273030). The eruption VEI (Volcanic Explosivity Index) marked on the top of dashed lines are from the eruptive history database of the Smithsonian Institution.

Fourier analysis has been used to determine the main frequency for each EEMD component of MODIS LST as shown in Figure 4. The dominant period on the original LST time series and its EEMD components (C1–C7) are the following: LST is about 5 years (1,747 days); C1 is around two months (64 days); C2 is around four months (134 days); C3 is around one year (318 days); C4 is around three years (1,165 days); C5 is around five years (1,747 days); C6 and C7 are around two decades (6,989 days). Time scales for each EEMD component are useful because they may imply the frequency of a certain physical phenomenon, and provide information for future eruptions in Mayon. Besides, we can only predict the volcano behavior to the extent of the near future (to the decadal time scale) depending on the available extent of LST time series.

The statistical significance test for information content of IMFs with unknown noise level has been proposed in previous studies (Barnhart and Eichinger, 2011; Wu and Huang, 2004). This test determines which IMF from MODIS LST (i.e., a noisy data set) contains information, and which IMF is merely noise. This test utilizes the statistical features of white noise which generally contains no information. The seven decomposed IMFs (C1–C7) are shown in Figure 5 along with the selected upper and lower confidence limit level (i.e., 99% and 1%

confidence limits). By comparisons on energy density of the IMF from the dataset, an IMF that has the energy located within the upper limit and the lower limit is considered to contain information at that selected confidence level. All IMFs marked as stars are within the 99 percentile confidence limit in Figure 5. Therefore, all IMFs are statistically different from white noise.

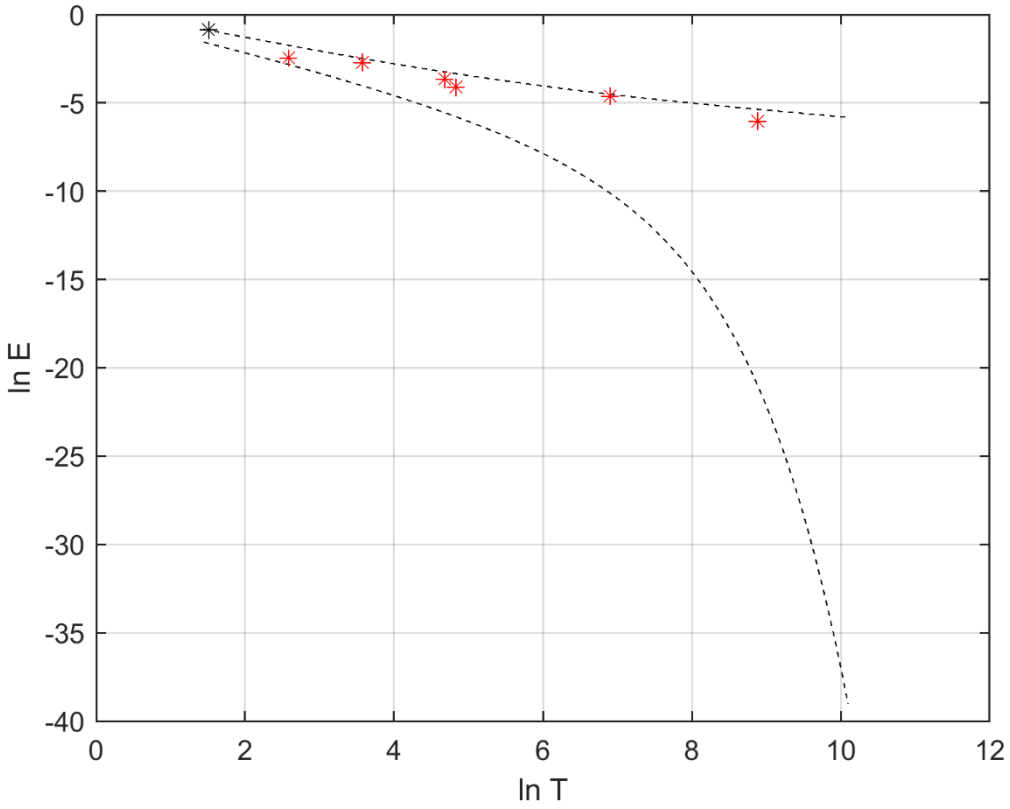

Figure 5. Statistical significance test for the extracted IMFs. Energy (E) of IMFs is a function of Period (T). The black color dashed lines are the first and 99th percentiles (1% and 99%) confidence level. Note that all the extracted IMFs marked by asterisks are within the confidence limits and are therefore considered statistically significant in their difference from noise. The black asterisk at the top-left corner represents the first IMF (C1).

These eight EEMD components (C1–C7, and Trend) were extracted from the MODIS LST time series of about 800 data points (463 data points are useful after screening). Each IMF is possibly related to a certain physical process. For example, component C3 with a 318-day (annual) period is similar to that of near surface air temperature. The annual cycle of air temperature is dominated by the insolation, season and vegetation. Both C1 and C2 (with period of about two and four months respectively) contain numerous irregular oscillation spikes. C4 of a three year period with lower amplitude possibly corresponds to the circulation of the atmosphere. C5–C7 exhibit amplitudes one order smaller than the other IMFs. C5 exhibits a five year timescale, C6 and C7 have periods in decadal timescales. The secular-up LST trend appears to gently increase from 2000 to 2019.

4. Discussion

4.1. Implications of LST Annual Period Component: Comparison with Air Temperature

The LST annual period EEMD component C3 (318-day period; around one year) is intimately connected with the on-site annual period near surface air temperature based on the period, i.e., 318-day vs. one year. A portion of LST components is contributed by the air temperature via the dynamics of land-air interactions in the surface energy balance process (Gallo et al., 2011). Thus the comparison analysis between the annual period LST and air temperature is very relevant and the result can be informative.

LST is the radiative temperature from the land surface. It is determined by heat contributions from either above or below the surface. An anomalously high heat-flow can be recognized on infrared images of the Earth's surface if the temperature at a depth of 0.5 m is about 50°–70°C or greater. It is calculated that the temperatures of 50°–70°C at 0.5 m depth are equivalent to heat-flow values of 8–30 watts per square meter (Wm^{-2}). This approximates 100–500 times the normal heat-flow (an average of about 80 mWm^{-2}) at the Earth's surface, but surface heat-flow values of 5–10 times the normal value may denote the presence of a subsurface thermal source in the area (Davies and Davies, 2010; USGS, 1995). In this study the general heat suppliers from beneath are geothermal (magma) resources and volcanic eruptions, while the heat contributors from above are the sunlight and air temperature. Part of LST components is corresponding to the near surface air temperature which is echoed through the annual variation derived by the Sun, season and vegetation. This part (i.e., LST annual period component C3) is regular and similar to the near surface air temperature time series. On the other hand, the irregular parts of LST components contain both the geothermal and volcanic causes. Among them, the geothermal contribution is generally consistent and regular for multi-decadal to millennial scale. However, volcanic unrest or eruptions are not consistent and their irregularity is likely to distort the regular pattern, such as the annual cycle. We thus infer from the above reasoning that the investigation of the annual period component C3 will facilitate our understanding and assessment of Mayon's behavior.

Figure 6 shows comparisons on the annual period LST component and air temperature. EEMD decomposed LST annual period component (C3) and the corresponding near surface (2 m height) on site air temperature are compared in more detail. We have detrended the on-site monthly air temperature and utilized it as an annual cycle reference. We have also calculated statistical Kurtosis and Skewness parameters for measuring the similarity level of the two time series. The kurtosis and skewness are numerical measures of shape: skewness indicates the asymmetry or distortion departure from a symmetrical bell curve, and kurtosis shows the height and sharpness of the central peak relative to a normal distribution, i.e, a normal distribution has skewness and excess kurtosis of 0 (Bulmer, 1979). If these two time series have high similarity, this signifies that the LST truthfully reflected the air temperature on the annual component. Higher similarity indicates lower heat contribution from the subsurface, such as volcanic unrest or eruptions. On the contrary, if these two time series have low similarity, this indicates that Mayon's LST annual period component is highly influenced by the volcanic events. The calculated Kurtosis and Skewness indicate low similarity of the two time series. Figure 7 gives a more comprehensive display of EEMD decomposed MODIS LST and the comparison between the LST annual period component and the monthly detrended on site air temperature in Mayon crater.

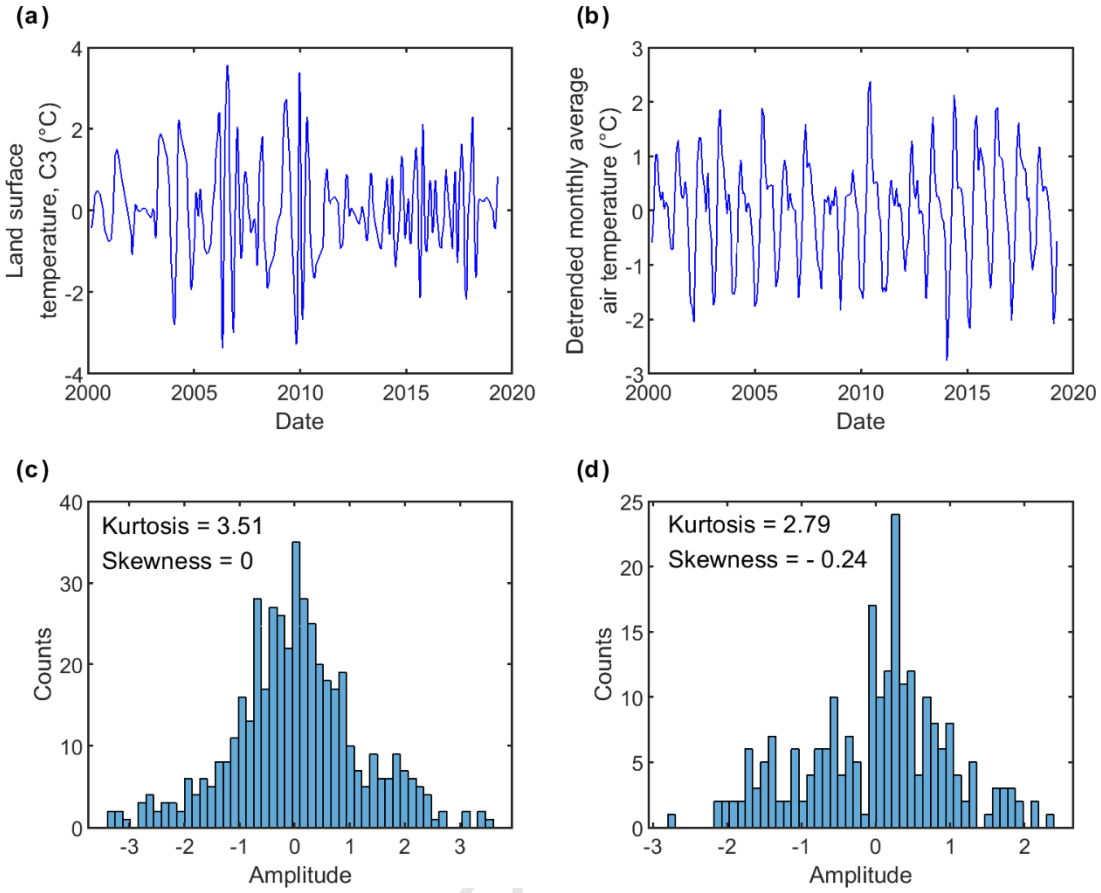

Figure 6. LST annual period component vs. annual cycle on site air temperature in Mayon crater. (a) and (c) are the LST EEMD annual component (C3) and its histogram. (b) and (d) show the on-site monthly detrended air temperature and histogram. The air temperature dataset is used for comparison. This dataset is provided by the NASA Prediction of Worldwide Energy Resource (POWER) and has a validated accuracy range of ± 0.96°C (Stackhouse Jr et al., 2018).

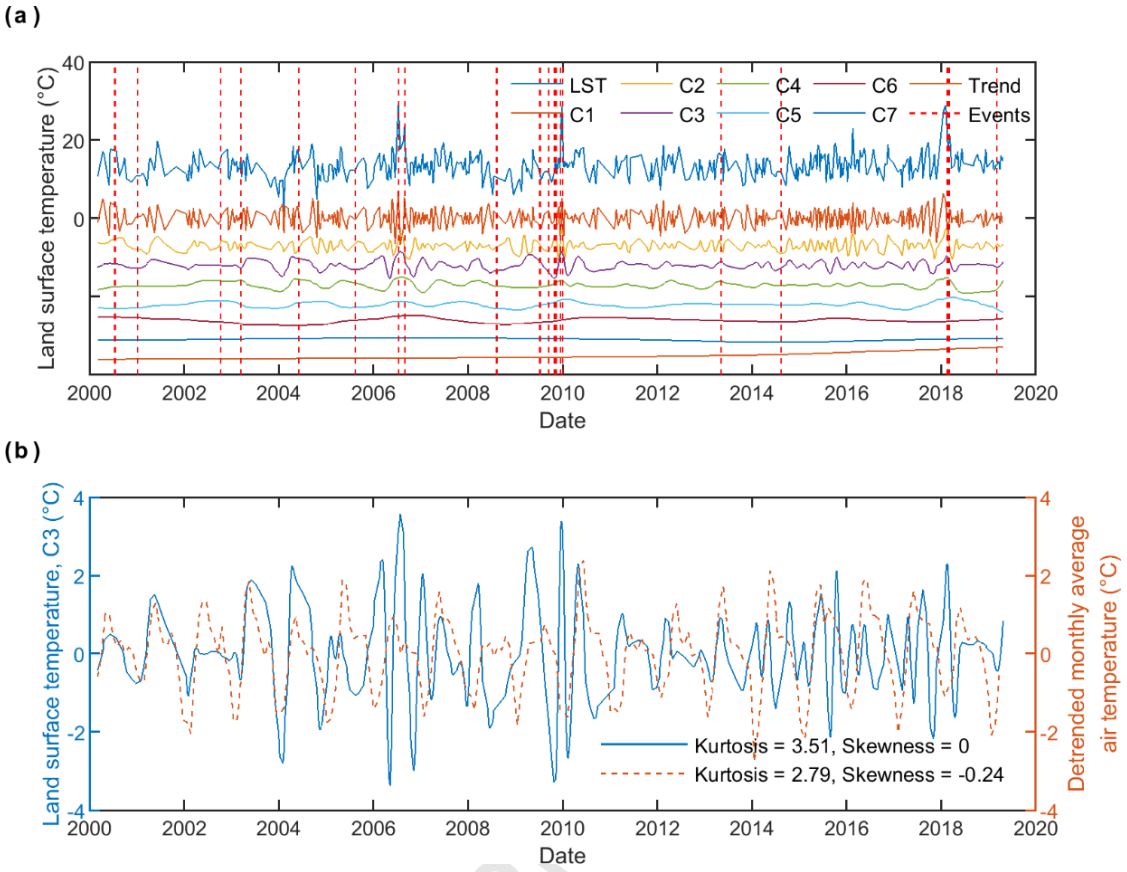

Figure 7. EEMD components of the MODIS LST at Mayon crater. (a) Decomposition of MODIS LST at Mayon crater from March, 2000–April, 2019. Volcanic unrests and eruptions are marked with red color dashed vertical lines. (b) Comparison of the annual period LST component and the monthly on site air temperature (detrended) at Mayon crater.

4.2. Characteristics of LST Components of Mayon Volcano

Increasing heat release is the most significant outcome of volcanic unrest or eruptions, and LST is most responsive to the heat released on the surface of the volcano. The characteristics of LST components of Mayon volcano are analyzed for further understanding of Mayon's future eruption trend. A few findings have been reached and listed below based on the EEMD analysis.

First, as shown in Figure 6 and Figure 7, the LST annual period component (C3) from Mayon volcano deviates from the regularity of annual cycle air temperature. The distortion from regularity is the result of eruptive activity. This fact implies that the dissimilarity between annual period LST component and site air temperature is a possible indicator of the restlessness level of the volcano.

Second, amplitudes of EEMD components with the shorter period such as C1 and C2 tend to increase with the volcano unrest or eruptions. In contrast, amplitudes of components with the longer period such as C4 and C5 (3-year and 5-year timescales) increase only with high intensity eruptions. A possible explanation is that the longer period components C4–C7 have amplitudes one order lower than others as shown in Figure 4. They usually reflect the longer term and larger scale fluctuation of the background. On the contrary, short period components record the short term or local scale variations of the environment.

Third, LST increases at Mayon crater may accompany the volcanic eruptions. However, the dependency of LST increases during the eruptions is not always clear. One reason is that the higher LST relies on the intensity and scale of eruptions. For the larger and fiercer erupting events, the LST response will be more obvious and vice versa. Another possible reason is the dataset deficiency for the period 2000 to 2019. LST observation dataset has gaps sometimes right before or after eruption events because of cloud coverage. Sharpness of LST curve indicates observation data sparsity in the time series as shown in Figure 3. This happens more frequently in geographic regions of humid tropical climates (e.g., Philippines) and moist

middle latitude climates because of higher water vapor content of air, which causes more cloud formation. Besides, the scale–mismatch effect on surface temperatures may also cause the discrepancy between the eruption and the high LST. Satellite derived LST is the average temperature within the pixel dimension. However, the dimension of volcanic craters is smaller than 200 m, on the contrary, the pixel size (spatial resolution) of MODIS LST images is 1 km.

Fourth, in EEMD decomposition approach, the LST time series is an aggregate or combination of these decomposed components (i.e., C1–C7, and Trend) as shown in Figure 4. Thus future trends of observed LST time series can be constructed easily by adding components of various timescales. Trends of different timescales based on the MODIS LST decomposition components at Mayon crater are shown in Figure 8. These trajectories basically all indicate the longer term secular-up trend, which means that Mayon volcano will remain restless in the future decades.

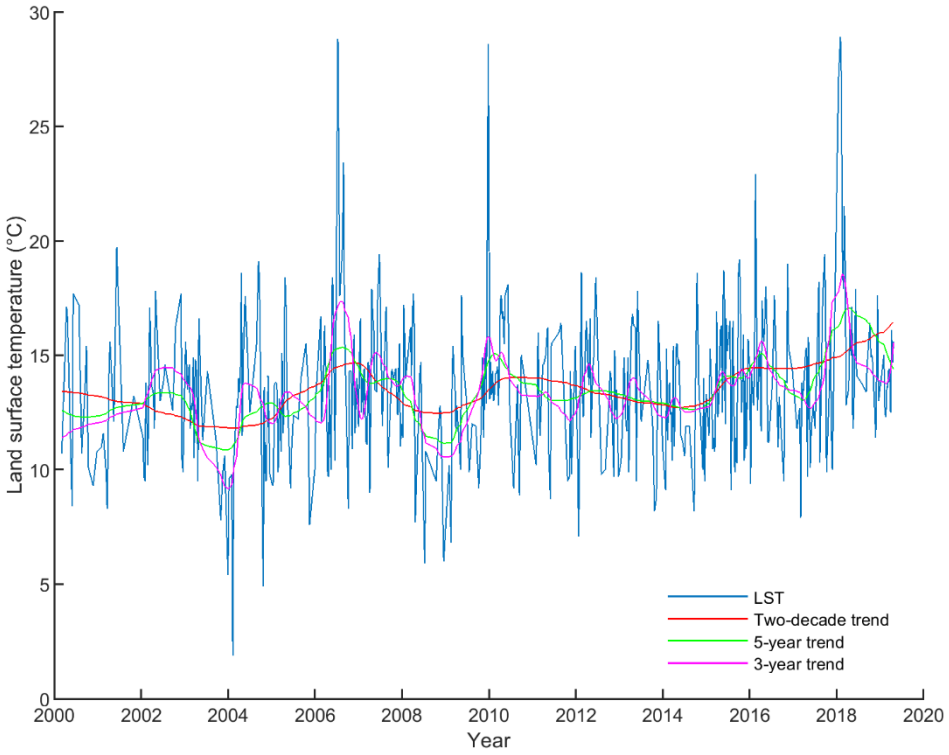

Figure 8. Trends of different timescales based on the MODIS LST decomposition components at Mayon crater. Note that the sum of the last three components (two-decade trend) of LST satisfies well the definition of trend.

4.3. Further validation: ASTER nighttime LST time series at Mayon crater

ASTER sensor is jointly managed by NASA and Japan's Ministry of International Trade and Industry. It is one of five imaging instruments flying on the Terra satellite launched in 1999 as part of NASA's Earth Observing System (NASA, 2020). ASTER aims to gather detailed data on surface temperature, emissivity, reflectance, and elevation at a relatively high spatial resolution (15 m – 90 m). ASTER is the solely high spatial resolution instrument on the Terra platform. It can be used in concert with the MODIS sensor which monitors the Earth at moderate to

coarse spatial resolutions. Owing to the higher spatial resolution, ASTER serves as a 'zoom' lens for the other instruments. It is particularly important for change detection, calibration/validation, and land surface studies. However, unlike the other instruments aboard Terra, ASTER does not collect data daily; it has a revisit time of 16 days. Therefore, the ASTER data sparsity is inevitable. ASTER gathers data in 14 different spectral bands of the electromagnetic spectrum, ranging from visible to thermal infrared light (i.e., visible and near infrared subsystem, short wave infrared subsystem, and thermal infrared subsystem). In this study, ASTER high-resolution (90 square meters per pixel) nighttime thermal infrared images of Mayon volcano are used to further validate the MODIS LST.

Figure 9 depicts the LST time series extracted from a total of 166 cloud free images (out of 246 available scenes) of 90 m spatial resolution ASTER nighttime Surface Kinetic Temperature (Product ID: AST_08v003) that were retrieved at the Mayon crater area (USGS, 2016). The purpose is to compare the 1 km spatial resolution 8-day average MODIS nighttime LST with the ASTER nighttime images at the study area. The two-decade trend of the ASTER LST time series is also illustrated. Results show that the MODIS LST products (in Figure 3) perform better than ASTER in this study. The total number of valid images in the study area from MODIS is about three times of ASTER. MODIS catches more thermal anomaly peaks caused by the eruptions than ASTER does because of its higher temporal resolution. The major advantage of MODIS is the subdaily acquisitions of images. Despite the lower spatial resolution, the higher temporal resolution does provide

more detailed land surface information of Mayon volcano. Both MODIS LST and ASTER LST time series (see Figure 8 and Figure 9) show the longer term secular-up trend. In addition, Table 1 lists the statistical summary on the retrieved land surface temperature at Mayon crater both from ASTER and MODIS sensors. It appears that MODIS acquired LSTs are generally 1–2 °C higher than those of ASTER. The discrepancy between ASTER and MODIS derived land surface temperatures can be attributed to the differences in spatial resolution and retrieval algorithms (Jacob et al., 2004; Liu et al., 2006). In general, the recorded secular-up trend of the MODIS LST time series is in agreement with the ASTER LST time series.

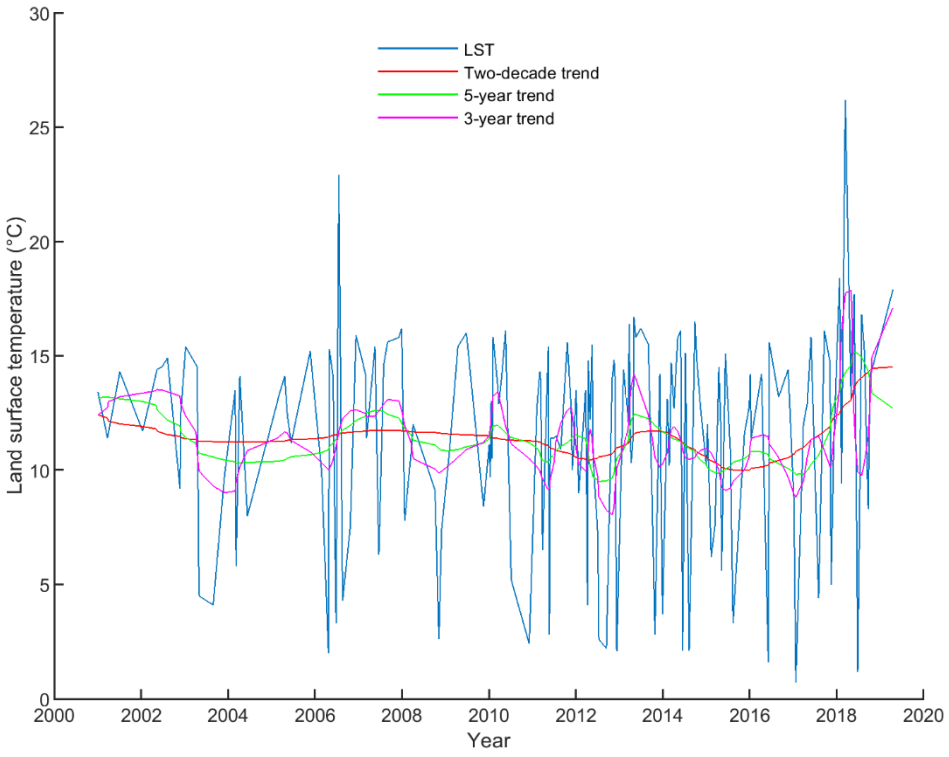

Figure 9. Illustration of the ASTER nighttime LST and its short-term and long-term trends at Mayon crater from January, 2001 to April, 2019.

Table 1. Statistical summary of land surface temperature at Mayon crater from ASTER and MODIS sensors (2000–2019).

Satellite & Sensor	Total number of valid images	LST (°C) Min	Max	Mean	Acquisition time (local time)
Terra ASTER	166	0.7	26.2	11.6	around 10:30 pm
Terra/Aqua MODIS	463	1.9	28.9	13.6	Terra: 10:30 pm Aqua: 1:30 am

5. Conclusions

Volcanic eruptions occurring near human habitats can affect lives and property. They pose a great threat to human life and infrastructure, causing death, destruction and environmental problems. Thus there is an urgent need to develop and expand reliable and affordable long-term methods in volcano monitoring.

This work uses the satellite derived multiscale and multitemporal surface temperature monitoring to validate the past eruptions and assess the future eruptive trend of Mayon volcano. Both ASTER and MODIS thermal infrared images were used to retrieve LST for delineating the thermal anomaly area of Mayon volcano, and EEMD method was used for decomposing nighttime 8-day average MODIS LST time series of Mayon crater. Physical processes related to EEMD components (i.e., C1–C7) have been explored. Specifically, the annual period component (C3; 318-day, around one year) is compared to regular annual cycle air temperature, the dissimilarity of the two time series has been taken as an indicator

of volcanic restlessness. Based on the comparison analysis on LST and air temperature annual oscillatory components, LST annual period component tends to lose its regularity if unrest or eruption occurs, and the dissimilarity level of the annual period LST component from the air temperature is an indicator of restlessness for active volcanoes.

The capabilities of thermal infrared remote sensing for mapping and quantifying surface thermal features and volcanic monitoring have been presented in this work. Results on applications of thermal infrared remote sensing enhance our knowledge for geothermal and volcanic areas. The proposed satellite-based monitoring approach not only helps to understand the eruptive potential of active volcanoes, but also provide valuable information for the understanding of subsurface volcanic structures, as well as volcanic effects and hazard mitigation. It can be applied to volcanoes where access is problematic, or when the volcanic monitoring budget is insufficient. It also works with the integration of the established monitoring systems to better study Mayon volcano as well as other volcanoes around the world.

With regard to volcano monitoring and hazard mitigation, it is expected that remote sensing will play an increasingly important role in hazard monitoring as more near real-time observations become available. Daily multiple high-resolution observations for thermal monitoring of volcanoes are required from a hazard mitigation perspective, since many of the satellites (e.g., Landsat, Terra, ENVISAT, ALOS, etc.) have repeat intervals of one day to about a month. Volcanic eruptions

are fast-developing phenomena and important eruption aspects may be missed by satellite sensors due to the long time interval between successive satellite overpasses (Mouginis-Mark, 2000). Despite such shortcomings, using satellite data for hazard mitigation and recovery remains a valuable option. Other strategies have to be developed by the remote sensing community and disaster managers to accommodate the need for high temporal and spatial resolution. For instance, applications of geostationary satellite data for real-time monitoring of volcanos (Ishii et al., 2018; Lombardo et al., 2019; Marchese et al., 2018) are making progress nowadays.

In essence, remote sensing cannot be expected to suffice as the sole tool for exploring and monitoring volcanoes since it is limited to detecting the surficial and the shallow buried geothermal features. Thus, an interdisciplinary approach, i.e., integration of geology, geophysics, geochemistry, and remote sensing will be the key to better understanding and application on prediction, hazard management, and assessment of volcanoes in the future.

Funding: This research was financially supported by the Ministry of Science and Technology (MOST) of Taiwan, grant number MOST 108-2116-M-008-011.

Acknowledgments: We would like to thank the Editor Diana Roman and two anonymous reviewers for their constructive comments. The ASTER images are available at https://lpdaac.usgs.gov/. The MODIS LST products are from the Global 1km level 3 MODIS Land Surface Temperature and Emissivity (LST/E) 8-day datasets (MOD11A2 Collection 6), available at

https://ladsweb.modaps.eosdis.nasa.gov/. The near surface air temperature products are provided by the NASA Prediction of Worldwide Energy Resource (POWER), available at https://power.larc.nasa.gov/index.php.

References

Barnhart, B.L. and Eichinger, W.E., 2011. Analysis of sunspot variability using the Hilbert–Huang transform. Solar Physics, 269(2): 439-449.

Bindhu, V., Narasimhan, B. and Sudheer, K., 2013. Development and verification of a non-linear disaggregation method (NL-DisTrad) to downscale MODIS land surface temperature to the spatial scale of Landsat thermal data to estimate evapotranspiration. Remote sensing of environment, 135: 118-129.

Blackett, M., 2013. Review of the utility of infrared remote sensing for detecting and monitoring volcanic activity with the case study of shortwave infrared data for Lascar Volcano from 2001–2005. Geological Society, London, Special Publications, 380: SP380. 310.

Blackett, M., 2015. An initial comparison of the thermal anomaly detection products of MODIS and VIIRS in their observation of Indonesian volcanic activity. Remote Sensing of Environment, 171: 75-82.

Bonafoni, S., 2016. Downscaling of Landsat and MODIS land surface temperature over the heterogeneous urban area of Milan. IEEE Journal of Selected Topics in Applied Earth Observations and Remote Sensing, 9(5): 2019-2027.

Bull, K.F. and Buurman, H., 2013. An overview of the 2009 eruption of Redoubt Volcano, Alaska. Journal of Volcanology and Geothermal Research, 259: 2-15.

Bulmer, M.G., 1979. Principles of statistics. Courier Corporation.

Castillo, P. and Newhall, C., 2004. Geochemical constraints on possible subduction components in lavas of Mayon and Taal volcanoes, southern Luzon, Philippines. Journal of Petrology, 45(6): 1089-1108.

Catane, S., Mirabueno, M., Listanco, E. and Solidum, R., 2001. Characteristics and origin of the pyroclastic flows and surges of the 1993 Mayon volcano eruption. J Geol Soc Philipp, 56(3–4): 125-143.

Chadwick, W.W., Archuleta, R.J. and Swanson, D.A., 1988. The mechanics of ground deformation precursory to dome-building extrusions at Mount St. Helens 1981–1982. Journal of Geophysical Research: Solid Earth, 93(B5): 4351-4366.

Chaussard, E. and Amelung, F., 2012. Precursory inflation of shallow magma reservoirs at west Sunda volcanoes detected by InSAR. Geophysical Research Letters, 39(21).

Cheng, C., Sa-Ngasoongsong, A., Beyca, O., Le, T., Yang, H., Kong, Z. and Bukkapatnam, S.T., 2015. Time series forecasting for nonlinear and non-stationary processes: A review and comparative study. Iie Transactions, 47(10): 1053-1071.

Davies, J. and Davies, D., 2010. Earth's surface heat flux, Solid Earth, 1, 5–24.

Davis, L.A., 2010. Natural disasters. Infobase Publishing, New York.

Delle Donne, D., Harris, A.J., Ripepe, M. and Wright, R., 2010. Earthquake-induced thermal anomalies at active volcanoes. Geology, 38(9): 771-774.

Ewert, J.W., Guffanti, M. and Murray, T.L., 2005. An assessment of volcanic threat and monitoring capabilities in the United States: framework for a National Volcano Early Warning System. Open-File Report 2005-1164, https://doi.org/10.3133/ofr20051164.

Flynn, L.P., Harris, A.J. and Wright, R., 2001. Improved identification of volcanic features using Landsat 7 ETM+. Remote Sensing of Environment, 78(1-2): 180-193.

Gallo, K., Hale, R., Tarpley, D. and Yu, Y., 2011. Evaluation of the relationship between air and land surface temperature under clear-and cloudy-sky conditions. Journal of applied meteorology and climatology, 50(3): 767-775.

Gupta, R.P., 2017. Remote sensing geology. Springer, Berlin, Germany.

GVP, 2013. Global Volcanism Program, 2013. Mayon (273030) in Volcanoes of the World, v. 4.8.5. Venzke, E (ed.). Smithsonian Institution. Downloaded 6 May 2019 (https://volcano.si.edu/volcano.cfm?vn=273030). https://doi.org/10.5479/si.GVP.VOTW4-2013.

Huang, N.E., Shen, Z., Long, S.R., Wu, M.C., Shih, H.H., Zheng, Q., Yen, N.-C., Tung, C.C. and Liu, H.H., 1998. The empirical mode decomposition and the Hilbert spectrum for nonlinear and non-stationary time series analysis, Proceedings of the Royal Society of London A: mathematical, physical and engineering sciences. The Royal Society, pp. 903-995.

Huang, N.E., Wu, M.-L.C., Long, S.R., Shen, S.S., Qu, W., Gloersen, P. and Fan, K.L., 2003. A confidence limit for the empirical mode decomposition and Hilbert spectral analysis. Proceedings of the Royal Society of London. Series A: Mathematical, Physical and Engineering Sciences, 459(2037): 2317-2345.

Huang, N.E. and Wu, Z., 2008. A review on Hilbert-Huang transform: Method and its applications to geophysical studies. Reviews of Geophysics, 46(2).

Huang, N.E., Wu, Z., Pinzón, J.E., Parkinson, C.L., Long, S.R., Blank, K., Gloersen, P. and Chen, X., 2009. Reductions of noise and uncertainty in annual global surface temperature anomaly data. Advances in Adaptive Data Analysis, 1(03): 447-460.

Ishii, K., Hayashi, Y. and Shimbori, T., 2018. Using Himawari-8, estimation of SO 2 cloud altitude at Aso volcano eruption, on October 8, 2016. Earth, Planets and Space, 70(1): 19.

Jacob, F., Petitcolin, F.o., Schmugge, T., Vermote, E., French, A. and Ogawa, K., 2004. Comparison of land surface emissivity and radiometric temperature derived from MODIS and ASTER sensors. Remote Sensing of Environment, 90(2): 137-152.

JICA, 2006. Japan International Cooperation Agency (JICA). JICA Report. The study on comprehensive disaster prevention around Mayon volcano, Part I: master plan. Land use planning. Retrieved 16 May 2020 from https://openjicareport.jica.go.jp/pdf/11603297_06.pdf.

Kisei, K., Satoshi, T., Corpuz, E., LAGUERTA, E., TUPPER, A., KANAGAKI, C., HAMADA, S. and IINO, N., 2008. Ground and satellite-based observations of Mayon volcano, Philippines. South Pacific Studies, 28(2): 53-68.

Liu, Y., Hiyama, T. and Yamaguchi, Y., 2006. Scaling of land surface temperature using satellite data: A case examination on ASTER and MODIS products over a heterogeneous terrain area. Remote Sensing of Environment, 105(2): 115-128.

Lombardo, V., Corradini, S., Musacchio, M., Silvestri, M. and Taddeucci, J., 2019. Eruptive Styles Recognition Using High Temporal Resolution Geostationary Infrared Satellite Data. Remote Sensing, 11(6): 669.

Maeda, Y., Kumagai, H., Lacson, R., Figueroa, M.S., Yamashina, T., Ohkura, T. and Baloloy, A.V., 2015. A phreatic explosion model inferred from a very long period seismic event at Mayon Volcano, Philippines. Journal of Geophysical Research: Solid Earth, 120(1): 226-242.

Marchese, F., Falconieri, A., Pergola, N. and Tramutoli, V., 2018. Monitoring the Agung (Indonesia) Ash Plume of November 2017 by Means of Infrared Himawari 8 Data. Remote Sensing, 10(6): 919.

Mouginis-Mark, P., 2000. Remote sensing observations for volcano monitoring and hazard mitigation. International Archives of Photogrammetry and Remote Sensing, 33(B7/3; PART 7): 905-910.

NASA, 2020. Terra Instruments. ASTER (Advanced Spaceborne Thermal Emission and Reflection Radiometer) Retrieved 16 May 2020 from https://terra.nasa.gov/about/terra-instruments/aster.

Nunes, J.-C. and Deléchelle, E., 2009. Empirical mode decomposition: Applications on signal and image processing. Advances in Adaptive Data Analysis, 1(01): 125-175.

PHIVOLCS, 2020. Philippine Institute of Volcanology and Seismology (PHIVOLCS). Eruption history of volcanoes, available at https://vmepd.phivolcs.dost.gov.ph/volcan/erupt-history.

Pyle, D.M., Mather, T.A. and Biggs, J., 2013. Remote sensing of volcanoes and volcanic processes: integrating observation and modelling–introduction. Geological Society, London, Special Publications, 380, 1-13, 25 September 2013, https://doi.org/10.1144/SP380.14.

Rivera, A.M.M., Amelung, F. and Eco, R., 2015. Volcano Deformation and Modeling on Active Volcanoes in the Philippines From ALOS InSAR Time Series, Fringe 2015 Workshop. European Space Agency.

Roberti, G., Ward, B., de Vries, B.v.W., Friele, P., Perotti, L., Clague, J.J. and Giardino, M., 2018. Precursory slope distress prior to the 2010 Mount Meager landslide, British Columbia. Landslides, 15(4): 637-647.

Slob, S., Fernandez-Alonso, M., Kervyn, F. and Bornas, M., 1998. Volcanic hazard mapping in the Philippines using remote sensing and GIS, Earth Surface Remote Sensing II. International Society for Optics and Photonics, pp. 54-66.

Stackhouse Jr, P.W., Zhang, T., Westberg, D., Barnett, A.J., Bristow, T., Macpherson, B., Hoell, J.M. and Hamilton, B.A., 2018. POWER Release 8.0. 1 (with GIS Applications) Methodology (Data Parameters, Sources, & Validation)

Documentation Date December 12, 2018 (All previous versions are obsolete)(Data Version 8.0. 1; Web Site Version 1.1. 0).

Tokunaga, M. and Thuy, V.T., 2000. Estimation of deformation volume in Mt. Mayon in Philippines using differential SAR interferometry by using EERS Tandem, IGARSS 2000. IEEE 2000 International Geoscience and Remote Sensing Symposium. Taking the Pulse of the Planet: The Role of Remote Sensing in Managing the Environment. Proceedings (Cat. No. 00CH37120). IEEE, pp. 2242-2244.

UNDRR, 2015. Volcano - Population Exposure Index (GVM). Retrieved 15 March 2020 from https://data.humdata.org/dataset/volcano-population-exposure-index-gvm.

USGS, 1995. Aerial Infrared Surveys in the Investigation of Geothermal and Volcanic Heat Sources. U.S. Department of the Interior, U.S. Geological Survey. Report 079-95. doi: 10.3133/fs07995.

USGS, 2013. Current Eruptions, Global Volcanism Program, the United States Geological Survey (USGS) and the Smithsonian Institution. Retrieved 6 May 2019 from https://volcano.si.edu/gvp_currenteruptions.cfm.

USGS, 2016. AST_08 v003. ASTER L2 Surface Kinetic Temperature. Retrieved 20 March 2020 from https://lpdaac.usgs.gov/products/ast_08v003/.

Wan, Z., 1999. MODIS land-surface temperature algorithm theoretical basis document (LST ATBD). Institute for Computational Earth System Science, Santa Barbara, 75.

Wan, Z., 2014. New refinements and validation of the collection-6 MODIS land-surface temperature/emissivity product. Remote Sensing of Environment, 140: 36-45.

Wan, Z. and Li, Z.-L., 1997. A physics-based algorithm for retrieving land-surface emissivity and temperature from EOS/MODIS data. IEEE Transactions on Geoscience and Remote Sensing, 35(4): 980-996.

Wang, Y.-H., Yeh, C.-H., Young, H.-W.V., Hu, K. and Lo, M.-T., 2014. On the computational complexity of the empirical mode decomposition algorithm. Physica A: Statistical Mechanics and its Applications, 400: 159-167.

Webley, P.W., Atkinson, D., Collins, R.L., Dean, K., Fochesatto, J., Sassen, K., Cahill, C.F., Prata, A., Flynn, C.J. and Mizutani, K., 2008. Predicting and validating the tracking of a volcanic ash cloud during the 2006 eruption of Mt. Augustine volcano. Bulletin of the American Meteorological Society, 89(11): 1647-1658.

Weng, Q., Fu, P. and Gao, F., 2014. Generating daily land surface temperature at Landsat resolution by fusing Landsat and MODIS data. Remote sensing of environment, 145: 55-67.

Westen, C.J.D., Arlene & Voskuil, Robert., 1994. Geomorphology of the mayon volcano and its relation to hazards. 10.13140/RG.2.2.11764.14723. Technical Report.

Wooster, M., Roberts, G., Smith, A., Johnston, J., Freeborn, P., Amici, S. and Hudak, A., 2013. Thermal infrared remote sensing: sensors, methods, applications.

Wright, R., Flynn, L., Garbeil, H., Harris, A. and Pilger, E., 2002. Automated volcanic eruption detection using MODIS. Remote sensing of environment, 82(1): 135-155.

Wu, Z. and Huang, N.E., 2004. A study of the characteristics of white noise using the empirical mode decomposition method. Proceedings of the Royal Society of London. Series A: Mathematical, Physical and Engineering Sciences, 460(2046): 1597-1611.

Wu, Z. and Huang, N.E., 2009. Ensemble empirical mode decomposition: a noise-assisted data analysis method. Advances in adaptive data analysis, 1(01): 1-41.

Zhang, E., Shan, D. and Li, Q., 2019. Nonlinear and Non-Stationary Detection for Measured Dynamic Signal from Bridge Structure Based on Adaptive Decomposition and Multiscale Recurrence Analysis. Applied Sciences, 9(7): 1302.

Author Statement

Conceptualization, H.-P.C. and K.K.;
Methodology, H.-P.C. and K.K.;
Software, H.-P.C.;
Validation, H.-P.C. and K.K.;
Formal Analysis, H.-P.C.;
Investigation, H.-P.C.;
Data Curation, H.-P.C.;
Writing—Original Draft Preparation, H.-P.C.;
Writing—Review and Editing, H.-P.C. and K.K.;
Visualization, H.-P.C.;
Project Administration, H.-P.C. and K.K.;
Funding Acquisition, H.-P.C. and K.K.

Disclosure statement

No potential conflict of interest was reported by the authors.

Highlights:

- Two-decade-long surface temperature at Mayon retrieved from MODIS and ASTER
- Components of various timescales extracted from the MODIS LST time series
- LST annual period component loses its regularity after eruptions
- Increasing secular trend points to future volcanic restlessness at Mayon